North Carolina Agricultural and Technical State University
Aggie Digital Collections and Scholarship

Theses | Electronic Theses and Dissertations

2011

Position Resolution And Efficiency Of The Lucite Hodoscope For The Sane Experiment At Jefferson Lab

John Henderson German
North Carolina Agricultural and Technical State University

Follow this and additional works at: https://digital.library.ncat.edu/theses

Recommended Citation

German, John Henderson, "Position Resolution And Efficiency Of The Lucite Hodoscope For The Sane Experiment At Jefferson Lab" (2011). *Theses*. 6.
https://digital.library.ncat.edu/theses/6

This Thesis is brought to you for free and open access by the Electronic Theses and Dissertations at Aggie Digital Collections and Scholarship. It has been accepted for inclusion in Theses by an authorized administrator of Aggie Digital Collections and Scholarship. For more information, please contact iyanna@ncat.edu.

POSITION RESOLUTION AND EFFICIENCY OF THE LUCITE HODOSCOPE FOR THE SANE EXPERIMENT AT JEFFERSON LAB

by

John Henderson German

A thesis submitted to the graduate faculty
in partial fulfillment of the requirements for the degree of
MASTER OF SCIENCE

Department: Physics
Major: Physics
Major Professor: Dr. Abdellah Ahmidouch

North Carolina A&T State University
Greensboro, North Carolina
2011

School of Graduate Studies
North Carolina Agricultural and Technical State University

This is to certify that the Master's Thesis of

John Henderson German

has met the thesis requirements of
North Carolina Agricultural and Technical State University

Greensboro, North Carolina
2011

Approved by:

Dr. Abdellah Ahmidouch Major Professor	Dr. Samuel Danagoulian Committee Member
Dr. Ashot Gasparian Committee Member	Dr. Abdellah Ahmidouch Department Chairperson

Dr. Sanjiv Sarin
Interim Dean of Graduate Studies

BIOGRAPHICAL SKETCH

John Henderson German was born on October 7, 1978, in Brooklyn, New York. During the beginning of his college years, he worked in the plant engineering field as a co-op student. He managed a small business in Greensboro, North Carolina for ten years before receiving his Bachelor of Science degree in Physics from North Carolina Agricultural and Technical State University in 2009. He was selected to be part of Hampton University Graduate Studies (HUGS) program. The College of Arts and Sciences awarded him the 2011 Merit Graduate Student Award. He is a candidate for the Master of Science degree in Physics.

ACKNOWLEDGEMENTS

It is with great pleasure to thank the many people who made this thesis possible. First and foremost I want to thank my advisor Abdellah Ahmidouch. I would have been lost without his encouragement, advice, teaching, and immense knowledge. He has made this journey worthwhile and enjoyable. Along with my advisor I would like to thank the entire Physics Department (staff and students) of North Carolina Agricultural and Technical State University. Their assistance, time, and energy were critical in the completion of this thesis.

The members of the Spin Asymmetry of the Nucleon Experiment analysis group contributed a great deal to the understanding of my research, and to them I am deeply indebted. It is with great pleasure for me to acknowledge my wife and children, Lakeisha, DeHondre, and Alexander, for their support and love throughout this process. To my family, friends, and all I've come in contact with, I offer my regards and blessings for without you there would have been no me.

TABLE OF CONTENTS

LIST OF FIGURES

FIGURES **PAGE**

LIST OF TABLES

TABLES **PAGE**

LIST OF ABBREVIATIONS

ADC	Analog to Digital Converter
ANN	Artificial Neural Network
BETA	Big Electron Telescope Array
CEBAF	Continuous Electron Beam Accelerator Facility
DIS	Deep Inelastic Scattering
DNP	Dynamic Nuclear Resonance
HMS	High Momentum Spectroscopy
PAW	Physics Analysis Workstation
PMT	Photomultiplier Tube
QCD	Quantum Chromo-dynamics
RSS	Resonance Spin Structure
SANE	Spin Asymmetries of the Nucleon Experiment
SSF	Spin Structure Function
TDC	Time to Digital Converter

ABSTRACT

German, John, Henderson. POSITION RESOLUTION AND EFFICIENCY OF THE LUCITE HODOSCOPE FOR THE SANE EXPERIMENT AT JEFFERSON LAB. **(Major Advisor: Abdellah Ahmidouch),** North Carolina Agricultural and Technical State University.

North Carolina A&T State University Nuclear Physics group built a Lucite Hodoscope, which was included in the Big Electron Telescope Array (BETA), to be used in the Spin Asymmetries of the Nucleon Experiment (SANE) at Jefferson Lab. SANE is a pioneering spin physics program that uses large non-magnetic detectors. SANE is a measurement of the proton spin observables $A_1^P(x,Q^2)$, $A_2^P(x,Q^2)$ and the spin structure functions (SSFs) $g_1^P(x,Q^2)$, $g_2^P(x,Q^2)$ over a Bjorken scaling variable x ranging from 0.3 to 0.8, covering the four-momentum transfer from 2.5 to 6.5 GeV^2. The experiment took place in Hall-C at Jefferson Lab. It will produce information about protons SSFs from an inclusive double polarization measurement. The role of the Lucite Hodoscope is to provide position information and enhance background reduction. This work studies the on beam performance of the Lucite detector through the recovery of its position resolution and efficiency.

CHAPTER 1

Introduction

The Lucite Hodoscope is a vital part of the Spin Asymmetries of the Nucleon Experiment (SANE) appartatus. North Carolina Agricultural and Technical State University (NCA&TSU) contributed the hodoscope to the experiment. The experiment took place at Jefferson Lab (JLab) and used the Continuous Electron Beam Accelerator Facility (CEBAF). The Lucite Hodoscope was constructed, tested, and installed by the NCA&TSU Nuclear physics group. It is a part of the Big Electron Telescope Array (BETA), which also included a Forward Tracking Hodoscope (Tracker), a N2 Gas Cherenkov (Cherenkov), and a Lead Glass Calorimeter (BigCal). BETA is the detector package for the experiment.

The SANE experiment main goal is to explore more into the proton's Spin Structure Functions (SSFs) from an inclusive double polarization measurement. The experiment ran from October 2008 to March 2009. The SANE experiment measured spin structure function $g_1^{\,p}(x,Q^2)$ and $g_2^{\,p}(x,Q^2)$ and proton spin asymmetry $A_1(x,Q^2)$ and $A_2(x,Q^2)$ at $2.5 < Q^2 < 6.5$ GeV^2 and $0.3 < x < 0.8$. From the SSF moments of g_1 and g_2 we hope to analyze the Twist-3 effects. From the measured g_2, we hope to study quark-gluon correlations and interactions.

The experiment was set up with the use of CEBAF's electron beam longitudinally polarized. The beam was scattered into a polarized proton target in both parallel and near perpendicular (80°) configurations. With the measured double spin asymmetries $A_{\parallel}$ and

$A_{\perp}$, we can evaluate proton spin asymmetries, A_1 and A_2, which will lead to structure functions, g_1 and g_2. Results can be compared with Lattice Quantum Chromo-Dynamics (Lattice QCD), QCD sum rules, bag model, and results of chiral symmetry. SANE measurements will fill the void of experimental data for the proton double spin asymmetry particularly in the kinematic range of Bjorken scaling variable $x > 0.3$ and $Q^2 < 6$ GeV^2 region.

The SANE experiment starts with electrons being sent into a proton target. CEBAF's beam line allows controlled polarized electrons to collide with a solid dynamically polarized NH_3 target. The scattered electrons are detected through BETA. Also recoiled protons can be detected by the High Momentum Spectrometer (HMS). Data collected from all detectors in the experiment will be analyzed.

This thesis will focus on the Lucite Hodoscope with emphasis on the analysis of its position resolution and efficiency. The Lucite is placed between the Cherenkov and BigCal. Its main purpose was to detect charged particles above a threshold (primarily electrons) with high efficiencies. Along with the detection of charged particles, it measured the coordinates and angles of scattered particles. The Lucite Hodoscope helps to trace the detected particles to the target. It provides useful information at reasonable cost.

Construction and initial testing of the Lucite bars took place at North Carolina Agricultural and Technical State University's Nuclear Lab. A team of students and professors conducted cosmic ray testing to check the performance of each Lucite bar. Satisfied with results from initial testing, the construction of the hodoscope commenced.

All 28 bars were individually wrapped in black opaque paper (tedlar) with photomultiplier tubes (PMTs) along with light guides attached to each end.

In understanding the Lucite Hodoscope, key physical concepts must be taken into consideration. The physics in Cherenkov radiation and internal reflection played critical roles calibrating and analyzing data. Devices such as PMTs, time to digital converters (TDCs), and analog to digital converters (ADCs) are attached to each detector to relay information for data acquisition. The computers at the facility stored the data and by accessing the network, analyzing programs were run. For data analysis and data visualization, the Physics Analysis Workstation (PAW++), a program from the Eurpoean Organization for Nuclear Research (CERN) program library, is used. PAW++ provides graphical presentation and statistical analysis by working with main objects or data types in the forms vectors, histograms and ntuples.

Large amounts of data collected from the experiment, is stored on tape silos at Jefferson Lab. Once the data is retrieved, it is analyzed through codes and stored in various forms. Fortran codes and Kumac scripts were used to calculate and graphically represent the collected data. Several codes work together for a large collection of data, while other codes are written just for specific goals. The results presented in this thesis are from codes partially written by the author, John Henderson German. Full analysis of the SANE experiment is ongoing and preliminary results of the $A_{\parallel}$ and $A_{\perp}$ asymmetries are reached.

CHAPTER 2

Physics Motivation

The Spin Asymmetry of the Nucleon Experiment (SANE) ran from October 2008 to March 2009. Many collaborators contributed to get information vital for further understanding on spin asymmetries of the proton. Its goals were to measure spin asymmetries, parallel and near perpendicular (80°) to the beam line, and structure functions over a range that has not been fully explored. It measured over a region of Bjorken scaling variable x from 0.3 to 0.8, for four-momentum, Q, transfers ranging from 2.5 to 6.5 GeV^2. The experiment made use of the high quality polarized beam of Jefferson Lab (JLab). It scattered longitudinally polarized electron beam from the Continuous Electron Beam Accelerator Facility (CEBAF) into a solid target dynamically polarized parallel and near perpendicular to the beam line. From these configurations, we were able to measure scattering asymmetries and precede to calculate physics asymmetries for the proton, $A_1(x,Q^2)$ and $A_2(x,Q^2)$, as well as the spin structure functions $g_1^{\,P}(x,Q^2)$ and $g_2^{\,P}(x,Q^2)$ where $x = Q^2/(2M\nu)$ with nucleon mass (M) and change in electron energy (ν).

Deep inelastic scattering (DIS) in this experiment is fundamental to probing inside hadrons. This inelastic electron-proton scattering allowed measured asymmetry values used to derive spin asymmetries for the proton. Calculating the spin structure functions allows access to higher twists. The formulation of equations for $g_1^{\,P}(x,Q^2)$ and $g_2^{\,P}(x,Q^2)$ leads to twist-3 contributions. For the high x region, there is little data on g_2.

These higher twist terms lead to information on quark-quark and quark-gluon coupling and interactions. Parallel configurations in this experiment led to g_1. Unfortunately, g_2 cannot be calculated with this model. The parton model limitations are apparent in scattering from transversely, near perpendicular, polarized targets. The higher twist effects cannot be ignored. In using the double spin asymmetries to calculate the spin structure functions, a model independent result can be used to improve the experimental dataset for A_1.

The measured double spin asymmetries $A_{\parallel}$ and $A_{\perp}$, are calculated by a combination of a dilution factor (f), average beam polarization (P_B), average target polarization (P_T), and the number of events recorded from the two different configurations ($N^{\uparrow\downarrow}$ and $N^{\downarrow\downarrow}$).

$$A_{\parallel} = A_{\perp} \cong \frac{1}{\mathrm{f} \cdot \mathrm{P_B} \cdot \mathrm{P_T}} \cdot \left(\frac{N^{\uparrow\downarrow} - N^{\downarrow\downarrow}}{N^{\uparrow\downarrow} + N^{\downarrow\downarrow}} \right)$$

The polarization of the electron at CEBAF Hall C is measured by a Moeller polarimeter. It consists of a polarized target, a magnetic channel with a combination of three quadruples and a detector made of lead glass and scintillators. The average target polarization is a calculated value from corrected online values. With these values, the calculation of the physics asymmetries A_1 and A_2 follows, with values for initial (E) and final (E') energies of electron, and the scattered electron's polar and azimuthal angles (θ and ϕ) respectively.

$$A_1 = \frac{1}{(E - E')} \cdot \left[(E - E' \cdot \cos\theta) A_{\parallel} - \left(\frac{E' \cdot \sin\theta}{\cos\phi} \right) \cdot A_{\perp} \right]$$

$$A_2 = \frac{\sqrt{Q^2}}{2 \cdot E} \cdot \left[A_{||} - \left(\frac{E - E' \cdot \cos\theta}{E' \cdot \sin\theta \cdot \cos\phi} \right) \cdot A_{\perp} \right]$$

There are several contributions from SANE. There is a lack on the proton double spin asymmetry $A_{\perp}$. Few points exist in the x > 0.3 and Q2 < 6 GeV^2 region with the exception of the Resonance Spin Structure (RSS) experiment at JLab [1, 2, 3]. The void in the data set around x=1, will significantly be improved from this model free result for A_1. Also, it will be compared to other predictions from SU(6), perturbative Quantum Chromo-Dynamics (QCD), and valence quark models[4]. Figure 1 denotes world data along with SANE expected data.

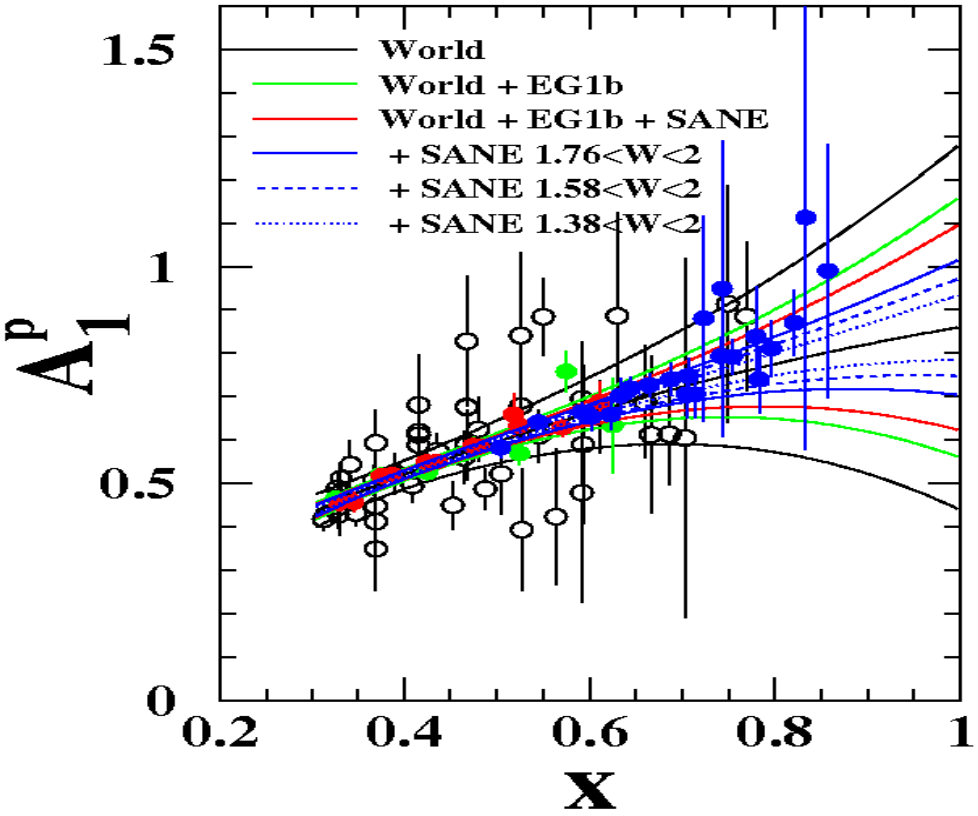

Figure 1. Expected A_1 data

The moments $g_1^P(x,Q^2)$ and $g_2^P(x,Q^2)$ allow calculation of higher twist terms. The experiment will compute the Nachtmann moments over the measured *x* range at several of constant Q^2, in combination with other data at neighboring kinematics [1, 2, 5]. The third Nachtmann moment of the combined g_2 and g_1, relevant to quark-gluon correlations, is related to the twist-3 reduced quark matrix element $d_2(Q^2)$ [6]. These correlations can be compared with the Handbag model [7, 8, 9], chiral soliton models [10, 11], lattice QCD [12], and QCD sum rules [13, 14]. Other important sum rules can be tested against the moments $g_1^P(x, Q^2)$ and $g_2^P(x, Q^2)$, such as the Burkhardt-Cottingham [15] and Efremov-Teryaev-Leader [16]. The Efremov-Teryaev-Leader sum rule must be tested using the measured g_1^P and g_2^P with neutron data from Hall-A in JLab.

These comparisons can be seen in Figures 2 and 3. Figure 2 shows expected results (statistical errors) for d_2 (open triangles), plotted on the expected pQCD evolution of d_2 (solid curve), normalized to Stanford Linear Accelerator Center, SLAC, C-N result (open circle) at 5 GeV^2. The solid square represents the RSS [1, 2, 3] results. The star indicates combined SANE results for $Q^2 = 5.2$ GeV^2. The lattice QCD calculation [12] (open square) is also shown. The elastic Nachtmann and C-N contributions are indicated by the dashed and dotted curves, respectively. Figure 3 shows comparison with Handbag model [7, 8, 9], QCD sum rules [13, 14], lattice QCD [12], and chiral quark soliton [10, 11].

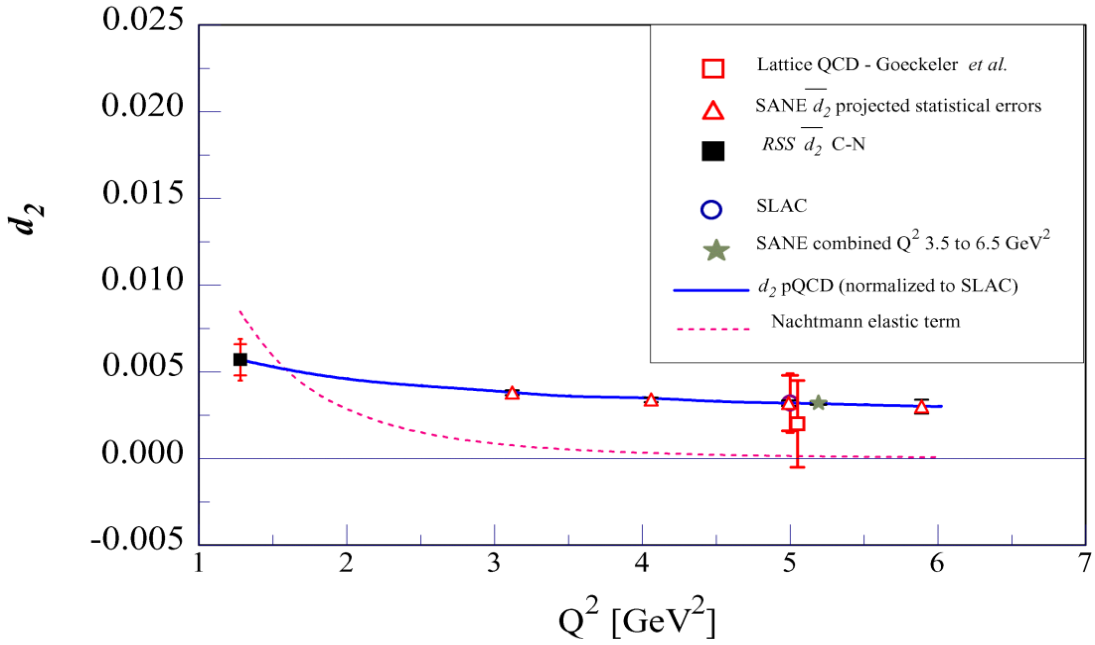

Figure 2. Expected d_2 results with statistical errors [1, 2, 3, 12]

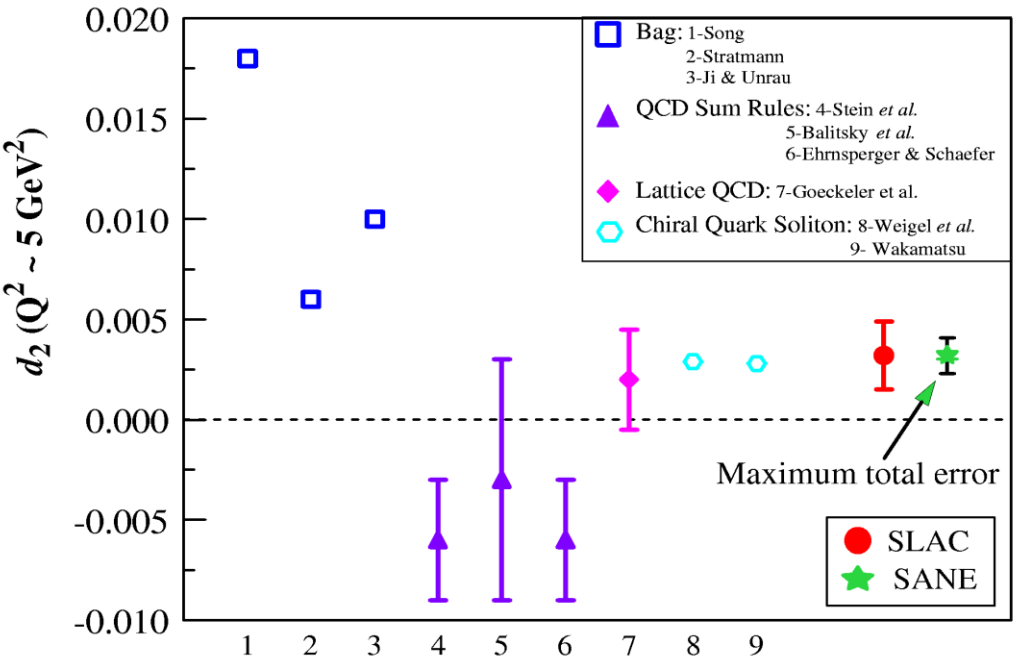

Figure 3. Expected d_2 results with comparisons to other models [7, 8, 9, 10, 11, 12, 13, 14]

From $g_1^{P}(x, Q^2)$ and $g_2^{P}(x, Q^2)$, the data can be used to test the x-dependence predicted by nucleon models.

$$g_1 = \frac{F_1}{1+\gamma^2} \cdot \left(A_1 + \gamma \cdot A_2 \right)$$

$$g_2 = \frac{F_1}{1+\gamma^2} \cdot \left(\frac{A_2}{\gamma} - A_1 \right)$$

$$\gamma = \frac{2 \cdot x \cdot M}{\sqrt{Q^2}}$$

Their Q^2 dependence at fixed *x* will be studied as well as the invariant mass of final states *W*. These spin structure functions are obtained from A_1, A_2, and the unpolarized structure function $F_1(x)$. These asymmetries and spin structure functions are quantities of interested needed to fill holes in previously measured experimental data. All of these conclusions will give SANE a chance to obtain a maximum amount of information on the nucleon spin structure of a proton.

CHAPTER 3

Experimental Set-up

The Spin Asymmetry of the Nucleon Experiment (SANE) was conducted in Hall-C at Jefferson Lab (JLab). Hall-C is one of the three existing experimental halls at JLab (currently JLab is building a fourth hall). The experiment setup included accelerator, beam line, polarized target, and the Big Electron Telescope Array (BETA). Figure 4 shows an aerial schematic where one can see the beam line enters from the right. The center of the figure shows BETA.

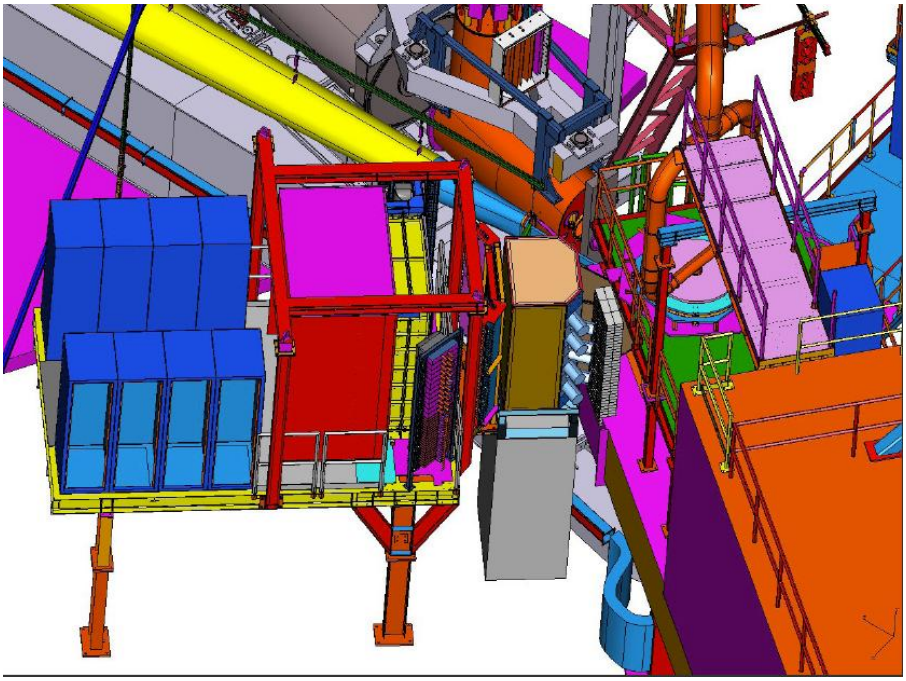

Figure 4. Aerial schematic of BETA

The vital part of Jefferson Lab is the Continuous Electron Beam Accelerator Facility (CEBAF). Figure 5 shows an aerial picture which indicates each part of the facility. This accelerator produces a beam with energy ranging from 0.8 to 6.0 GeV^2. It is a 5-pass continuous wave electron accelerator. Once the electron wave is injected, the electrons gain energy by going through cavities. Cavities are hollow shells made from niobium that allow electrons to gain energy by placing negative charges behind them and positive charges in front of them. Jefferson Lab's accelerator uses 338 cavities with microwaves directed into the cavities to push the electrons. The beam line sits in a tunnel that is 7/8 mile around, with two linear accelerators each about 1/4 mile long. Magnets are used to steer, focus, and defocus the electron beam. The beam current range is a few pA to 180 μA with position stability +/- .1 mm.

University of Virginia (UVa) contributed the target, used in the SANE experiment. The UVa target assembly used frozen solid Ammonia (NH_3) as well as Carbon (C) for background estimation. The target is polarized using Dynamic Nuclear Polarization (DNP). The principle of DNP is to enhance the low temperature (1 K) high magnetic field (5 T) polarization of solid materials by microwave pumping. DNP employs paramagnetic radicals, which provide electron-proton hyperfine splitting in a high magnetic field at moderate-low temperatures.

Figure 5. Aerial picture of CEBAF

The assembly housed two 3 cm targets that can be remotely selected. The target cells were kept in liquid Helium (He) and maintained at a temperature of 1 K. By exposing the target to 140 GHz microwaves we can polarize the target up to 95%. Polarized targets are necessary due to the experiment looking into the measured spin asymmetries of polarized leptons colliding with polarized nuclei. By being polarized, the spins of the protons or nuclei are all aligned in one direction. Also, the electron beam is polarized as well. So being able to control and manipulate the targets polarization we can achieve the sought after goal.

The High Momentum Spectrometer (HMS) is QQQD configuration, three quadrupoles (Q), magnets, and a dipole (D). The detector package is contained in a concrete shield house. The spectrometer detector was used only for background measurements, particle identification, and calibration purposes. After the beam hits the target, some of the scattered particles are focused onto this detector. It consists of several instruments that measure different elements of the particle: two wire chambers for particle measurements, scintillator hodoscopes for timing, gas Cherenkov for particle identification and calorimeter for energy measurement. The hodoscope contains two planes. Each plane in the hodoscope contains scintillator paddles with Photo Multiplier Tubes (PMTs) on both ends. This provides fast triggering. In the Gas Cherenkov there are two mirrors (top and bottom) and two PMTs in the focal planes. At the end there is a Lead-Glass Calorimeter that is 4 layers of 10 x 10 x 70 cm^3 blocks stacked 13 in each layer. The HMS detected deflected protons ejected from the target by the electron beam.

There are four major parts to the BETA detector package, the Forward Tracker (Tracker), N_2 Gas Cherenkov (Cherenkov), Lucite Hodoscope (Lucite), and a Lead-Glass Calorimeter (BigCal) shown in Figure 6. The Lucite detector is located between the Cherenkov and the BigCal approximately 255 cm from target. The BETA package sits at about 40° to the beam line. Due to limitations of space in the construction of SANE, a perpendicular angle of the target polarization could not be reached. The experiment will record parallel and near perpendicular (80° off beam line) configurations of the target polarization.

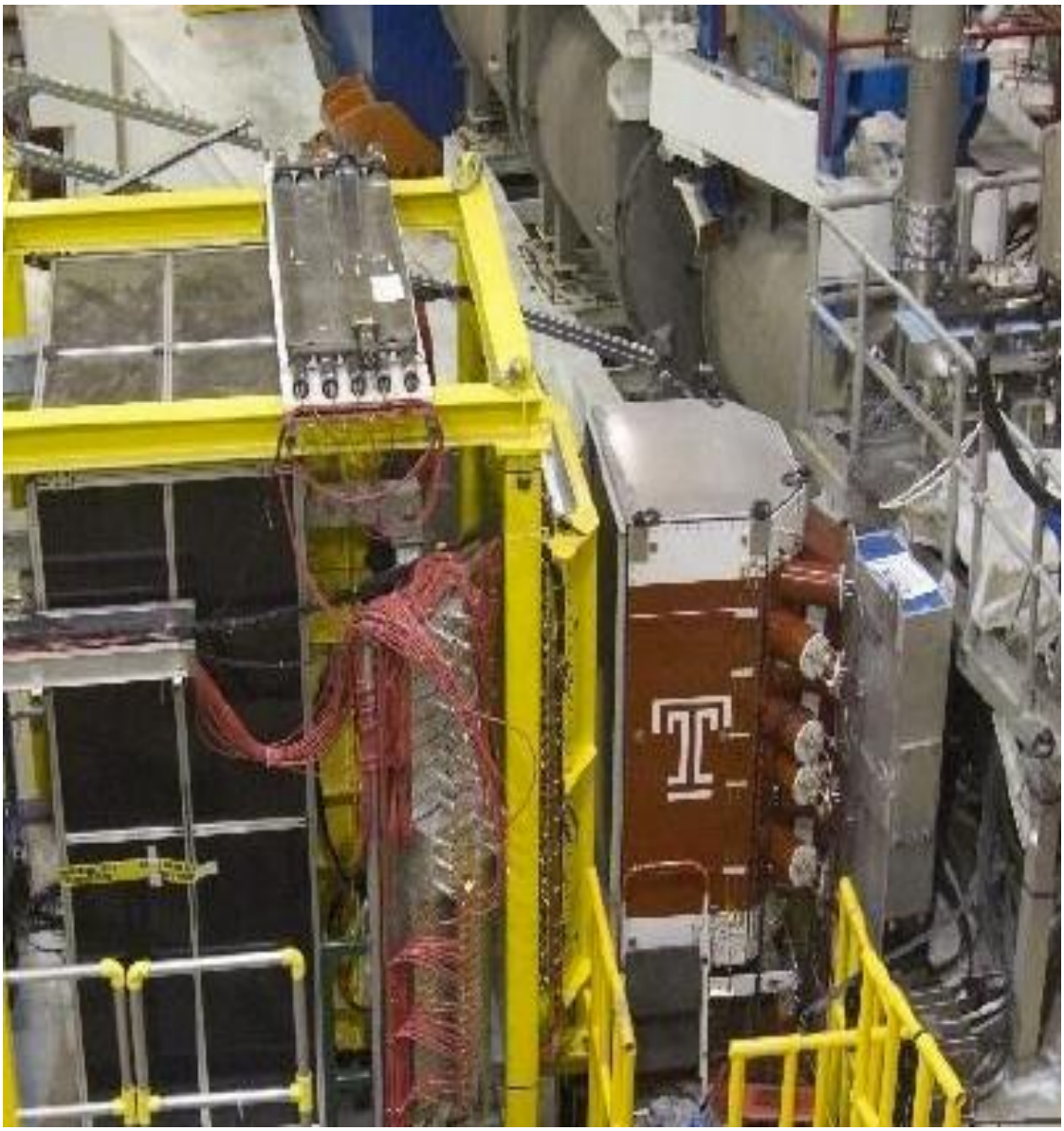

Figure 6. BETA in Hall C

Norfolk State University contributed the forward tracker. This is the metal box at the far right of BETA in Figure 6. It consisted of three planes of Bicron plastic Scintillator located 50 cm from target. The first plane is considered the X plane while the last two are the Y1 and Y2 planes. These planes give us early position measurement

close to the target field. The schematic in Figure 7 shows the orientation of the planes in Tracker.

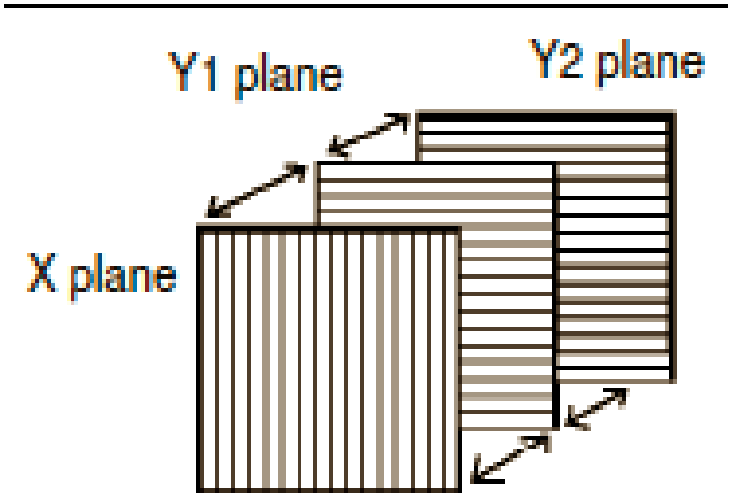

Figure 7. Forward Tracker schematic

Temple University provided the N_2 Gas Cherenkov, easily distinguishable fully attached to BETA because of the Temple logo on its side. It has 4 spherical and 4 toroidal mirrors with 8 3" PMTs. The detector is efficient in electron detection and pion rejection 1000:1. Cherenkov provided particle ID. The detector is shielded for 50:1 magnetic field reduction. Charged particles entering the detector produce Cherenkov radiation while moving through the N_2 gas with an efficiency of 90%. Pions are below threshold and are rejected with a ratio 1000:1. Figure 8 shows Cherenkov before connecting to BETA.

Figure 8. Gas Cherenkov

North Carolina A&T State University furnished the Lucite hodoscope sandwiched between the Gas Cherenkov and BigCal. Lucite is a relatively inexpensive material used to detect charged particles with good efficiency and provide useful position resolution at a reasonable cost. The detector has 28 Lucite BC-800 [17] bars with dimensions 3.5 x 6.0 x 96.7 cm^3. The bars are curved with the radius of 240 cm, to provide normal incidence of particles from the target. Bars are individually wrapped in black optical paper to ensure total internal reflection of the produced Cherenkov light. The edges of the bars are cut at 45 degrees to avoid reflections. A light guide made of Lucite is used to bring the light to a 2" PMT. Bars were oriented horizontally for Y tracking while the PMTs on both sides are used to determine X information.

A magnetic shielding box housed the PMTs of the Lucite hodoscope to protect them from the magnetic field surrounding the target. The hodoscope was affixed to BETA. The curved Lucite bars were fitted with rectangular to circular dimensioned light guides in order to attach a PMT to each end of the bars. Each PMT used is a Photonis XP2268 [18]. Figure 9 shows the schematic of an individual bar. Figure 10 shows three Lucite bars unwrapped with light guides attached. Figure 11 shows the fully constructed hodoscope from the view of the target without the last bar, before inserting into BETA.

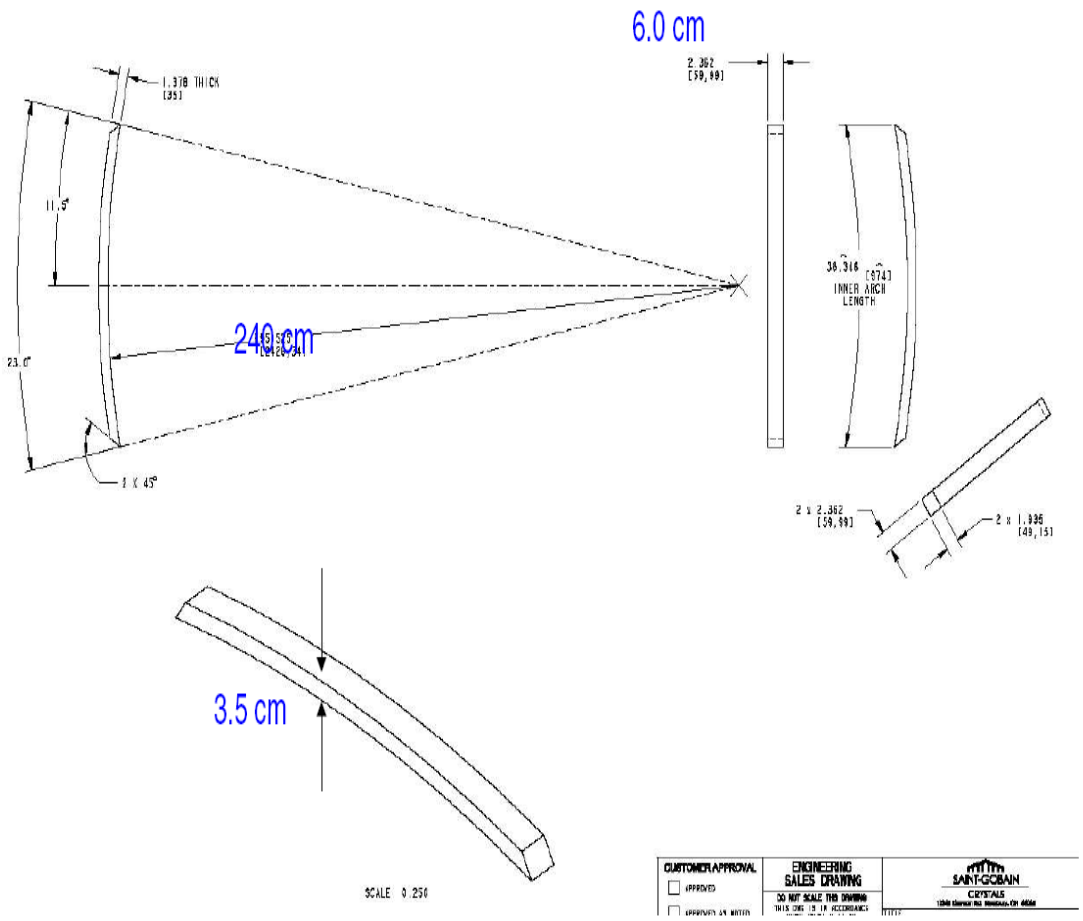

Figure 9. Schematic of Lucite bar

Figure 10. Three Lucite bars with light guides

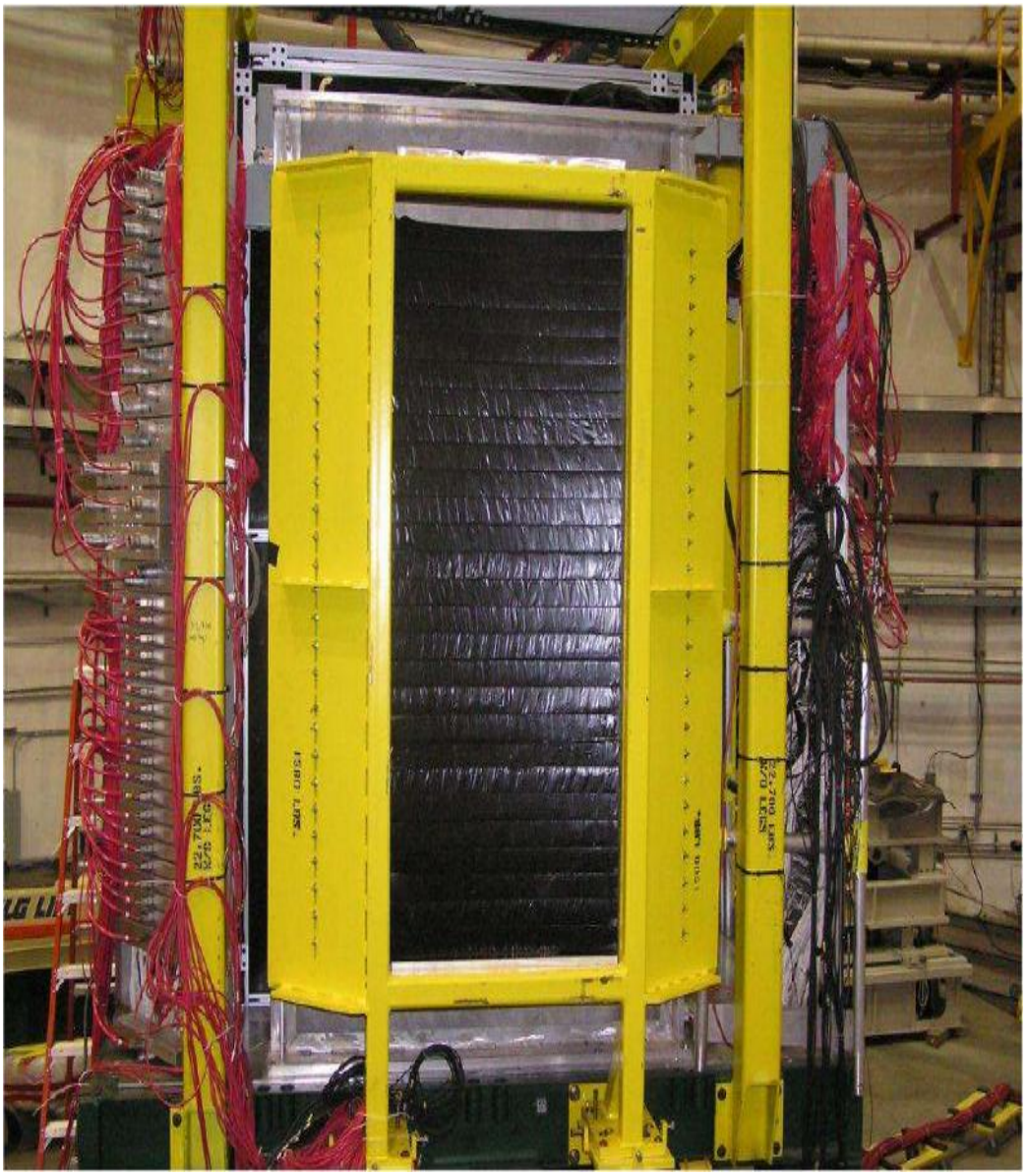

Figure 11. Fully constructed Lucite Hodoscope

Cables were attached to each PMT. One provided high voltage. The second was used to extract the signal to be processed by electronics and the data acquisition system. TDC, ADC, and coincidence units are used to process the PMT signals. TDCs are used to convert a signal of sporadic pulses into a digital representation of their time indices.

To convert signal amplitudes to discrete numbers, an ADC is used. The coincidence unit is used to record the events where both bar PMTs are giving a signal. The shielding box of the detector helped support the immense weight of the cables and shielded the detector from external magnetic field coming from the Helmholtz coil in the target.

The BigCal calorimeter is a collaboration project by the Institute for High Energy Physics (IHEP) Protvino, the College of William and Mary (W&M), and Lanzhou University. BigCal is the final destination for the particles. It records energy deposited by electron as well as position of the particle. It has 1744 lead glass bars. Each bar is 4 x 4 x 40 cm^3. They are stacked and fitted with a PMT on the ends. All together they are 56 blocks tall x 30-32 blocks wide (218 x 210 cm^2). Figure 12 shows a close view of BigCal.

Figure 12. Close up of BigCal

CHAPTER 4

BETA Detector Array

The Big Electron Telescope Array (BETA), which was a non-magnetic detector package, was an important part of the Spin Asymmetry of the Nucleon Experiment (SANE). BETA is composed of four parts; a Forward Tracker Hodoscope (Tracker), Gas Cherenkov (Cherenkov), Lucite Hodoscope (Lucite), and a Lead-Glass Calorimeter (BigCal). Each serves a purpose varying from background reduction to energy and position measurements. The Lucite Hodoscope is located between Cherenkov and BigCal. The design of the hodoscope allows for determination of position information. The hodoscope is used for tracking particles through BETA.

After scattering of the target, particles are ejected through the forward tracker hodoscope. They travel through three planes of 3 mm wide Bicron Scintillator to assist in early particle tracking. The first is denoted as the X plane and the others are in the order of Y1 and Y2. This combination indicates how the particle travels immediately after collision and just before entering the gas Cherenkov detector. The Nitrogen Gas Cherenkov detector is used to detect electrons and reduce the pion background. The produced Cherenkov light is reflected by the eight mirrors onto PMTs to provide particle identification. In order to have a reduction factor of 1000:1, the threshold for pion momentum is set up to 5.9 GeV^2/c.

Exiting the Cherenkov detector, particles pass through the Lucite Hodoscope. The movement through the bars produce Cherenkov radiation. This radiation is emitted

when a charged particle moves through a transparent medium faster than the speed of light in that medium. As the charged particles pass, photons are emitted similar to the sonic boom of a supersonic aircraft. These photons travel in a photonic shock wave through the bars. Due to total internal reflection, the photons are collected and measured by PMTs attached to the ends.

Photomultiplier Tubes are extremely sensitive detectors of light in the visible range of the electromagnetic spectrum. PMTs have high bandwidth and noise free gain on the order of a million, with ultra-fast response. They are ideal for the detection of extremely low light or short pulses light. Some photomultipliers can be used to detect photons from 115nm to 1700nm. The photons emitted from Cherenkov radiation have wavelength less or around 400nm. A typical photomultiplier consists of a photo emissive cathode (photocathode) followed by an electron multiplier and an electron collector (anode). The detectors can multiply the signal produced by incident light by as much as 10 million times. Photomultipliers are constructed from a glass envelope with a high vacuum inside.

The PMTs attached to the Lucite bars received a ratio of about 10 photoelectrons from the 40 to 50 Cherenkov photons in the visible range. The photons reflected into the PMTs passed though the input window. Then the light excites the electrons in the photocathode so that the photoelectrons are emitted into the vacuum through a process called external photoelectric effect. These photoelectrons are accelerated and focused by the focusing electrode on the first dynode where they are multiplied by means of secondary electron emission. This process is repeated at each of the successive dynodes.

The multiplied secondary electrons emitted from the last dynode are collected by the anode.

The PMTs magnified 10 photoelectrons to around $10^7 - 10^8$ photoelectrons. This signal is sent to the Time to Digital Converter. The TDC received input from both ends of the Lucite bars. The computer records the time difference in the PMTs. The threshold speed of the particle inside the Lucite bars can be determined from Cherenkov radiation and total internal reflection angles. With the index of refraction of Lucite: n = 1.49 and Cherenkov radiation angle $\theta_c > 43°$, the speed of the particles, $\beta = .9176$, is calculated from the following relationship.

$$\cos\theta = \frac{1}{n \cdot \beta}$$

By having the speed of the particle calculated, the horizontal position can be analyzed with those values and the time differences in the left and right PMTs in the following equation, where c is the speed of light in bars, n is the index of refraction, θ is the total internal reflection angle, and *offset* is an coefficient based off each bar.

$$X_{position} = (TDC_{Left} - TDC_{Right}) \cdot \frac{c}{n} \cdot \cos\theta_{TIR} - offset$$

With 28 Lucite stacked vertically, the vertical position can be determined by identifying the bar which is hit and its position.

Once the particles exit the bars, they are detected in BigCal and deposit its full energy. BigCal was located 335 cm from the target. It consists of 1792 elements of optically isolated lead glass blocks stacked in rows. It is used for energy and position determination of the electrons. The impact of an electron onto BigCal causes a shower of

radiation surrounding that element. Accurate determination of position and energy is derived from the resultant cluster. Figure 13 is a schematic for the path of travel through BETA for a particle. The dotted line travels through the Tracker, then Cherenkov, Lucite, and finally ends up in BigCal.

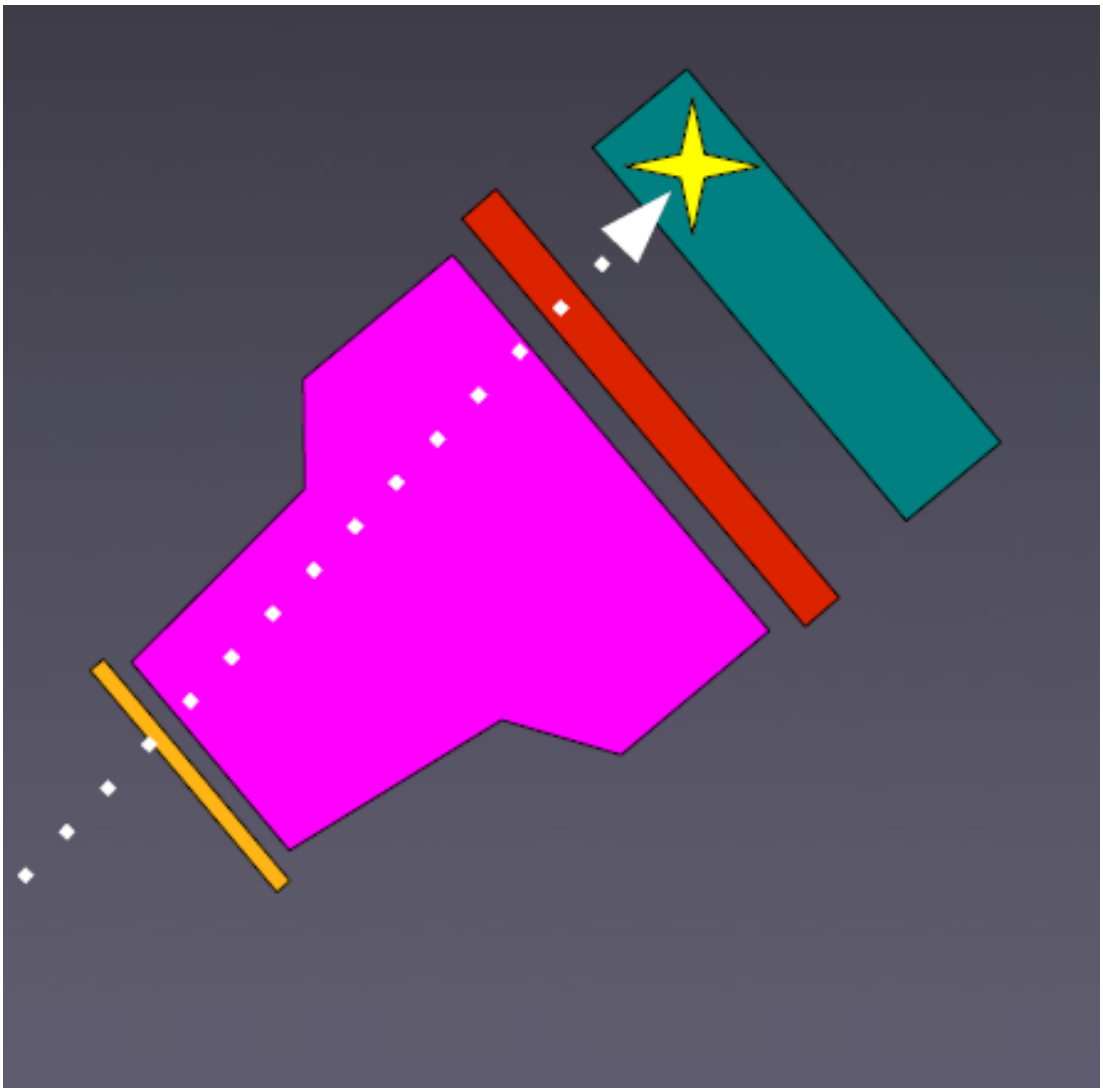

Figure 13. Path through BETA

CHAPTER 5

Analysis of Lucite Performance

With the use of different computational software packages and programming languages, the analysis of the Spin Asymmetry of the Nucleon Experiment (SANE) has begun. Computer simulation of the Big Electron Telescope Array (BETA) with GEANT3, from the European Organization for Nuclear Research program library, allows comparison between experimental and simulated data. GEANT (GEometry ANd Tracking), a software package originally used for high energy experiments, uses Monte Carlo methods to produce results. For determination of Lucite efficiency and position resolution, PAW++ (Physics Analysis Workstation) was used with Fortran codes and Kumac scripts. This chapter focuses on the Lucite Hodoscope data analysis.

Due to all the data collected during SANE, many cuts were used to filter out unnecessary data. For the analysis of the Lucite Hodoscope (Lucite), every part of BETA was taken into consideration. On the Forward Tracker Hodoscope (Tracker), acceptable events were ones that hit all three planes and position could be determined. For the Gas Cherenkov, the momentum threshold rejects particles of no interest especially pions. Events with energies greater than 1 GeV^2 and less than 6 GeV^2 were selected by the Lead-Glass Calorimeter (BigCal). Some particles hit multiple Lucite bars during its travel through BETA. Figure 14 shows the multiplicity comparison of events that hit one Lucite bar compared to two and three Lucite bars.

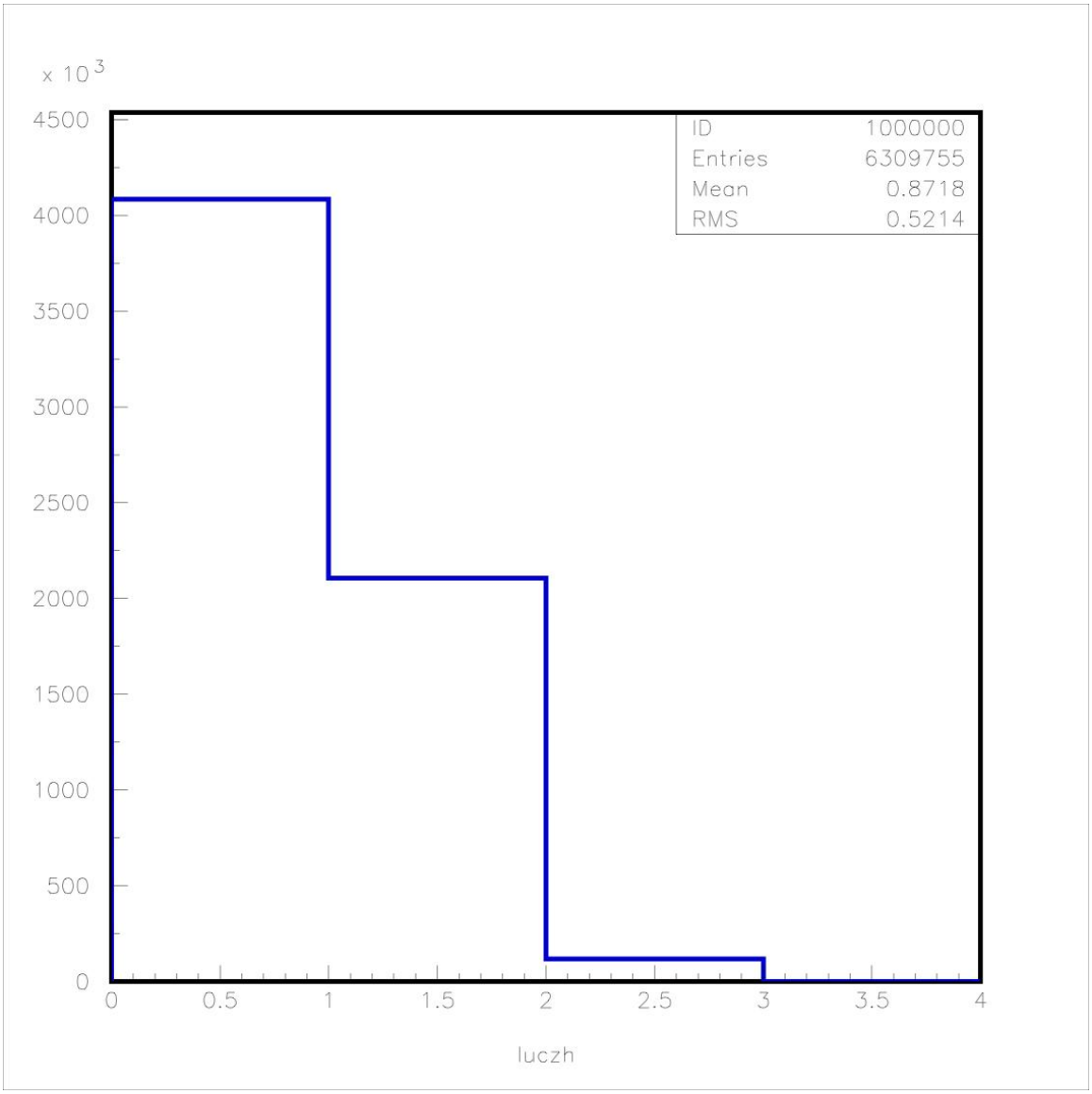

Figure 14. Lucite hit multiplicity

The Forward Tracker Hodoscope provides initial position and the start of the trajectory. With one plane oriented horizontally and two vertically, the path from the target through the three planes is well defined. The final destination of the particles was the BigCal. In order to improve accurate cluster position and energy deposition, a

technique called Artificial Neural Network (ANN) was used. The SANE GEANT Monte Carlo set of data were used to train the ANN algorithm. The algorithm uses the energy of the clusters and patterns in BigCal to more accurately determine horizontal and vertical coordinates as well as the particles energy. Figure 15 shows Narbe Kalantarians work with ANN. The figures show considerably improved coordinate and energy resolution.

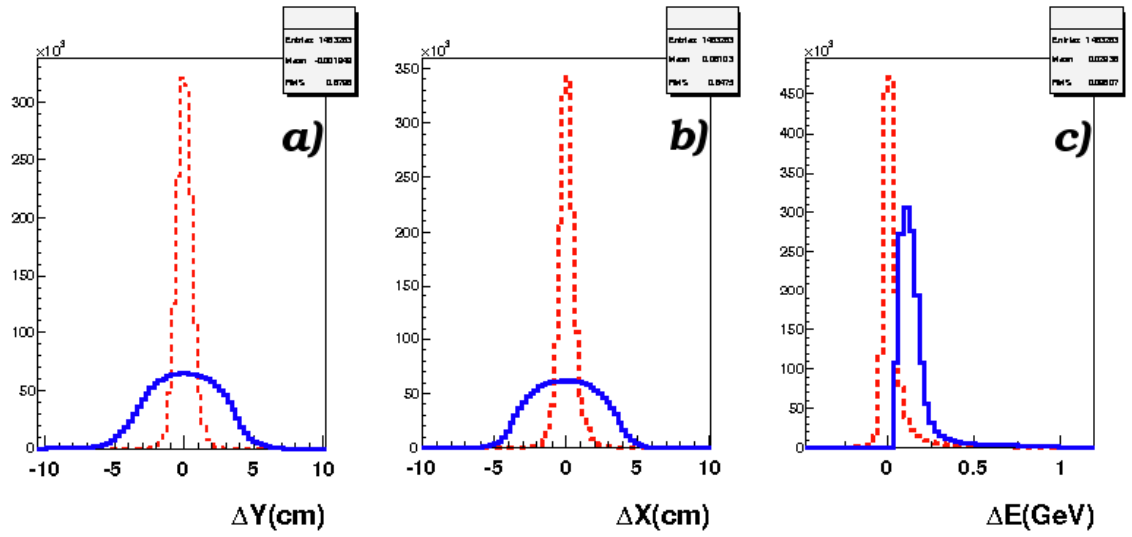

Figure 15. Differences in generated and reconstructed coordinates and energy using conventional (solid blue curve) and ANN (dashed red curve) methods

The horizontal (X) and vertical (Y) predicted values are calculated separately. With accurate initial (X_1, Z_1) and ending positions (X_2, Z_2), reconstruction of the predicted trajectory follows. Two accurate points will produce a line with a given slope by the following formula.

$$slope = \frac{X_2 - X_1}{Z_2 - Z_1}$$

The predicted X value is determined by the following formula.

$$X_{predicted} = \left[X_1 - \left(slope \cdot Z_1\right)\right] + \left(slope \cdot 255\right)$$

For predicted Y values, the same procedure was followed.

These predicted values are compared to measured values from data received during the experiment as shown in the previous chapter. The Lucite's recorded X position was calculated from the difference in Time to Digital Converters (TDC) values for the PMTs on each side of the bar along with constants such as speed of light in Lucite, index of refraction in material, and angle of reflection inside the bars. Other parameters were determined during calibration such as timing shifts and coefficients that were different for each bar. The values for speed of light in the bars, index of refraction of Lucite, and cosine of the angle of reflection, total internal reflection angle, are 2.99×10^8 m/s, 1.49, and 0.7313 respectfully.

In order to analyze efficiency and position resolution, several confirmations had to be gained. Graphs should coincide with known values and configurations. Noticeable in Figure 16 are the scattering of events over the hodoscope as well as the distinction of each of the 28 bars. One can also see and measure the curvature of the hodoscope in the graph of the X-Z plane. The needed linear relationships between data collected on the Lucite hodoscope and BigCal can be seen in Figure 17. This 2-D plot also shows the majority of hits occurring on one side.

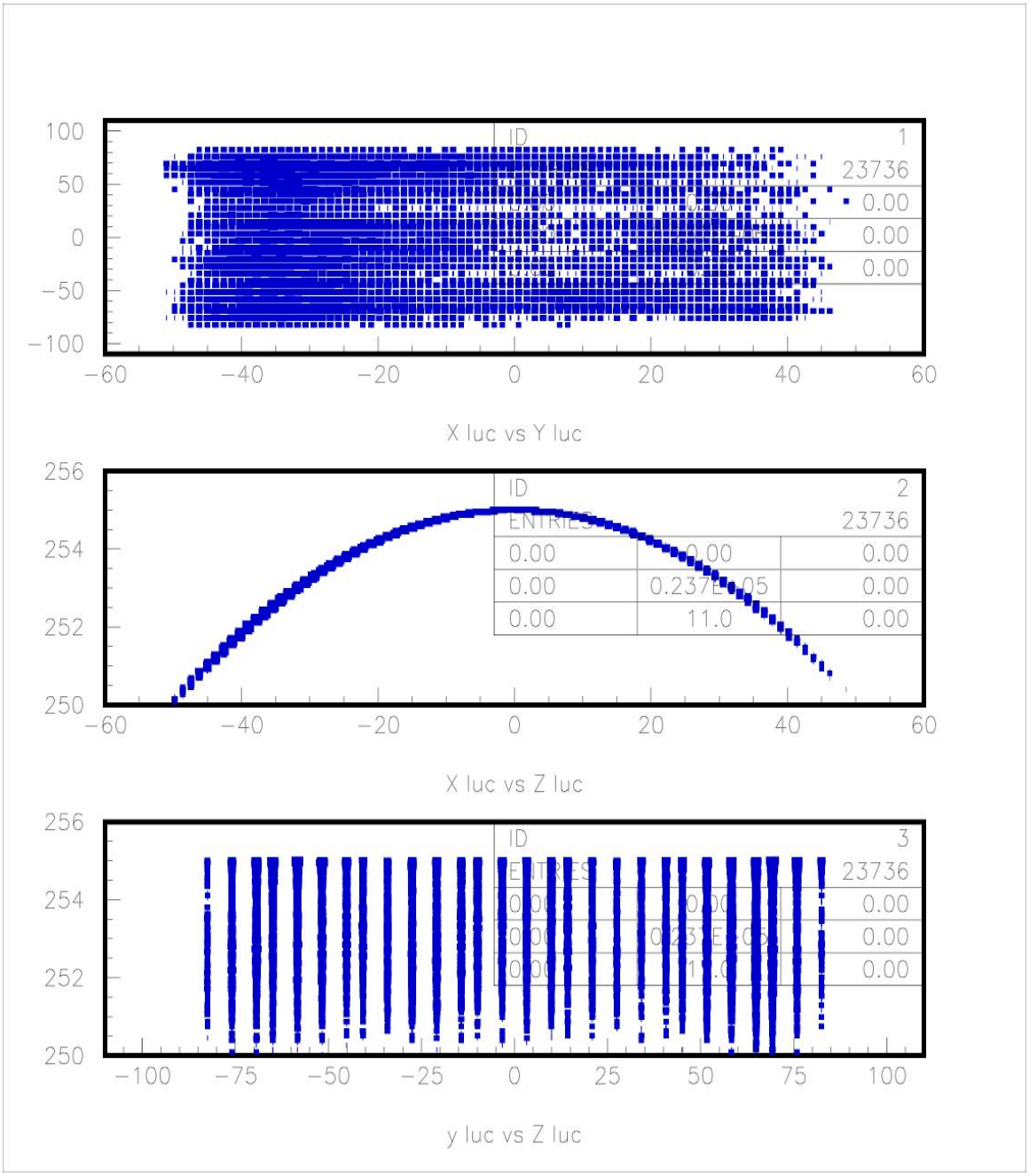

Figure 16. X vs. Y, X vs. Z, and Y vs. Z

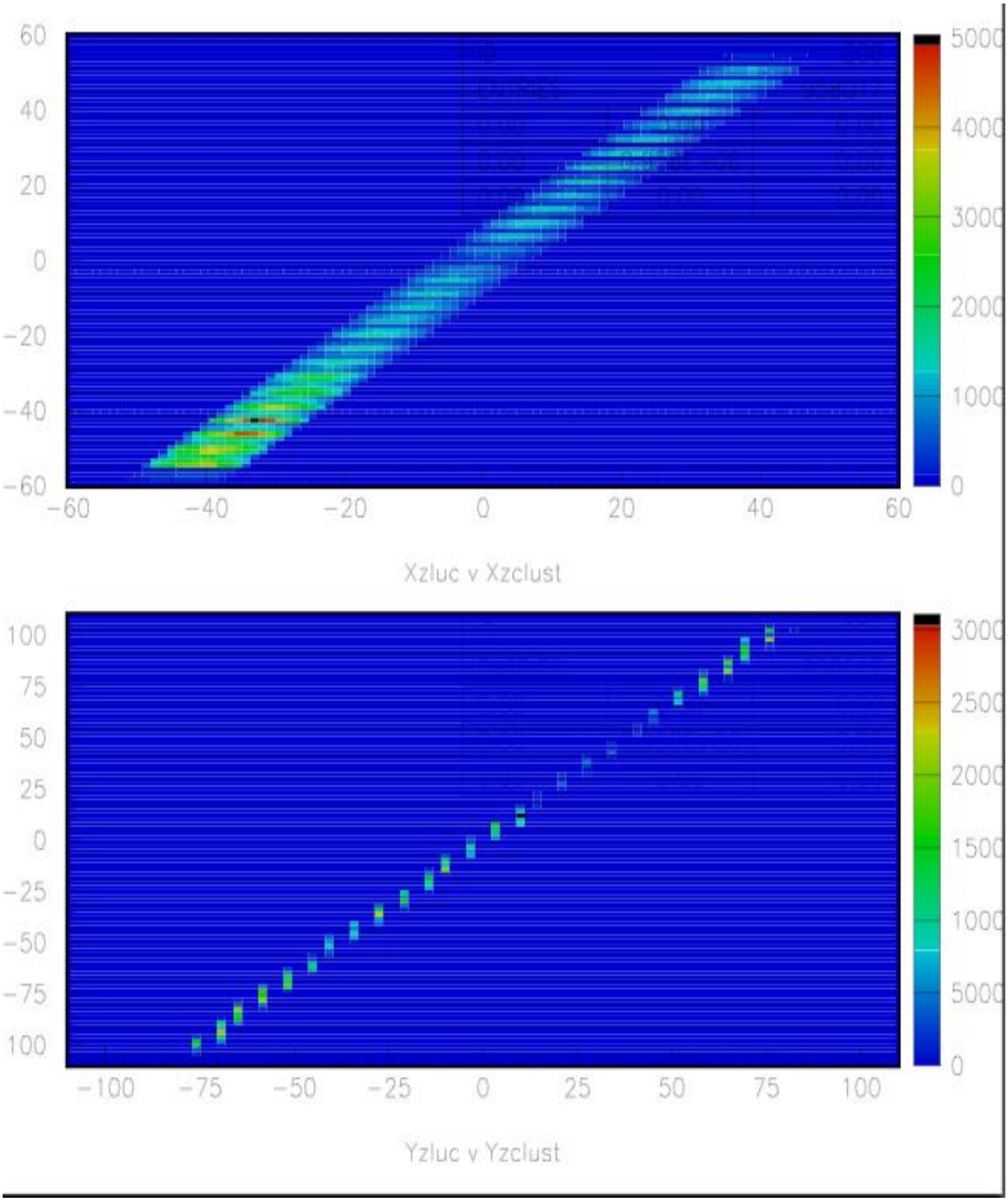

Figure 17. 2-D graph of Lucite vs. BigCal

Once confidant with recorded values, calculation of predicted values from experiment can begin. By knowing two points the particle traveled through, we algebraically predict where it hit the Lucite hodoscope. With these predicted values, global efficiency of the hodoscope can be calculated as well as efficiency per bar. Table 1 shows a table of the values for global efficiency. Figure 18 shows histograms of collected data events and predicted events on all bars viewed on the X plane as well as the global efficiency derived from the ratio of the two. Dividing the total number of events detected in the experiment after cuts by the predicted amount detected we get a global efficiency around 56%.

Before taking the bars to JLab for SANE experiment, efficiency was found to be around 90%. Collaborators in the experiment believe that because of the process of adding the hodoscope into BETA, which included bending and cutting the bars, the efficiency dropped. Many agreed that the global efficiency would be around 56%. Table 2 shows the efficiency per bar in horizontal sections. Looking at efficiency per bar, Figures 19-21, low efficiencies can be found at the top and bottom of the hodoscope while more consistent values are seen towards the middle.

Table 1. Global efficiency

Distance across bar in cm	-50 to -30	-30 to -10	-10 to 10	10 to 30	30 to 50
Percentages	59.2	61.0	53.8	58.7	51.5

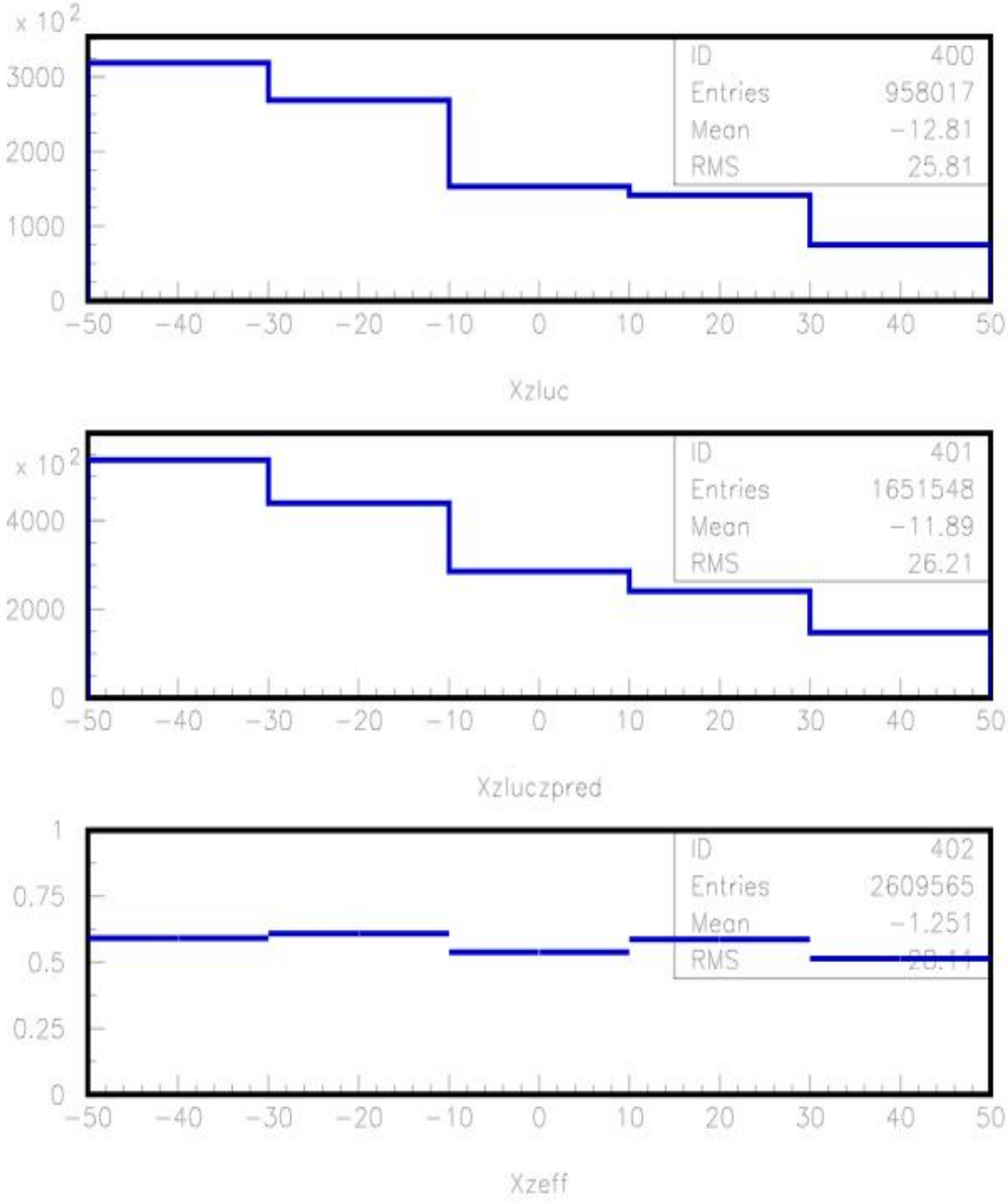

Figure 18. Lucite collected and predicted values with efficiency

Table 2. Efficiency per bar

Bar	-50 to -30cm	-30 to -10cm	-10 to 10cm	10 to 30cm	30 to 50cm
1	31%	31%	11%	2%	0%
2	29%	31%	28%	32%	40%
3	****	74%	45%	50%	70%
4	53%	58%	52%	74%	****
5	56%	67%	59%	49%	55%
6	88%	81%	63%	64%	42%
7	83%	89%	92%	97%	93%
8	68%	47%	47%	48%	39%
9	36%	59%	57%	50%	29%
10	65%	63%	51%	49%	64%
11	68%	64%	75%	72%	98%
12	57%	49%	39%	43%	33%
13	87%	78%	70%	66%	****
14	****	70%	48%	91%	79%
15	45%	45%	41%	36%	61%
16	****	89%	89%	70%	71%
17	95%	72%	30%	72%	71%
18	67%	51%	62%	58%	52%
19	50%	56%	35%	53%	33%
20	83%	56%	48%	66%	63%
21	27%	48%	35%	52%	46%
22	63%	50%	32%	35%	57%
23	36%	35%	39%	45%	14%
24	53%	53%	46%	68%	54%
25	52%	60%	43%	57%	46%
26	65%	55%	44%	39%	49%
27	****	****	76%	****	54%
28	****	****	****	****	****

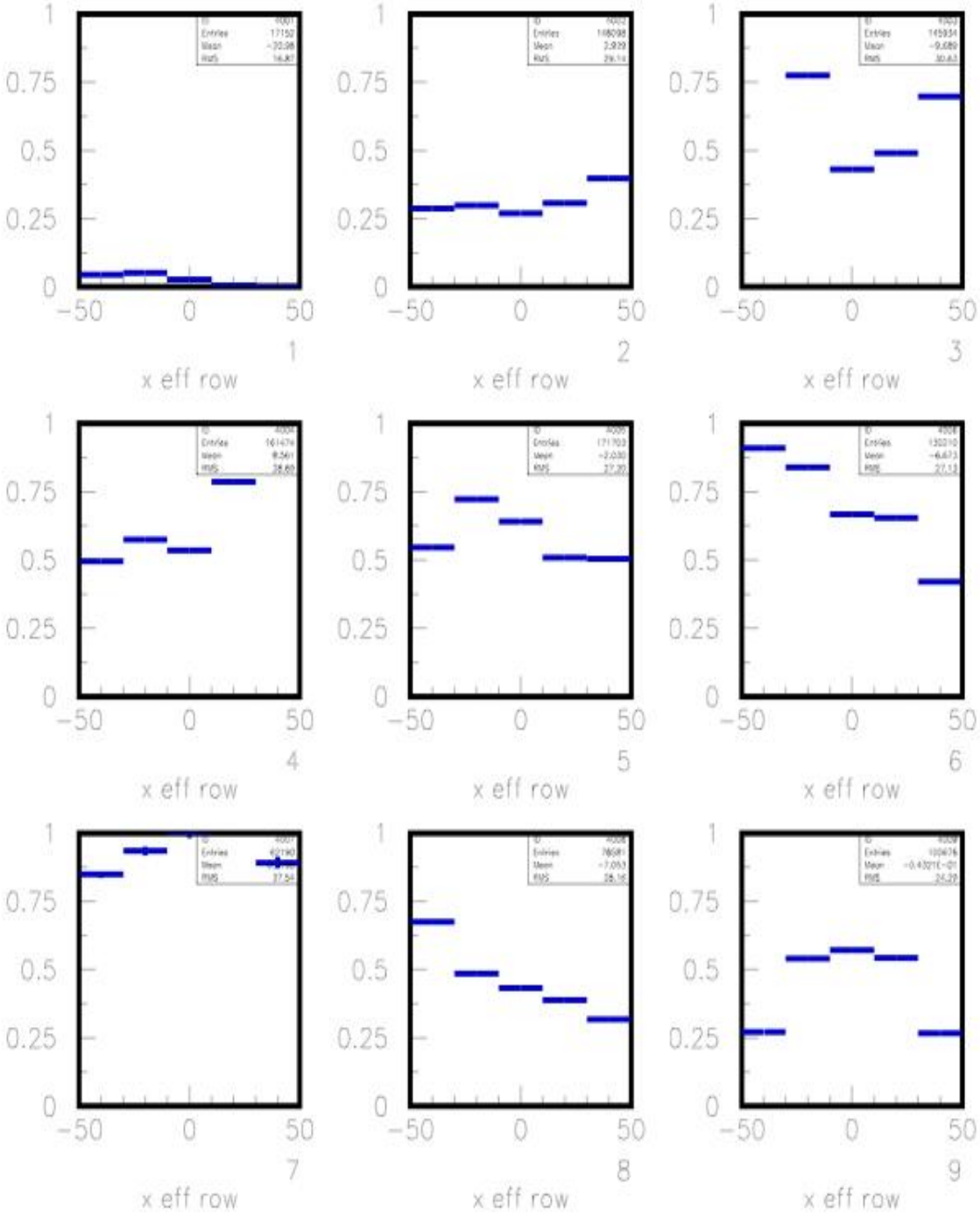

Figure 19. Per bar efficiency 1-9

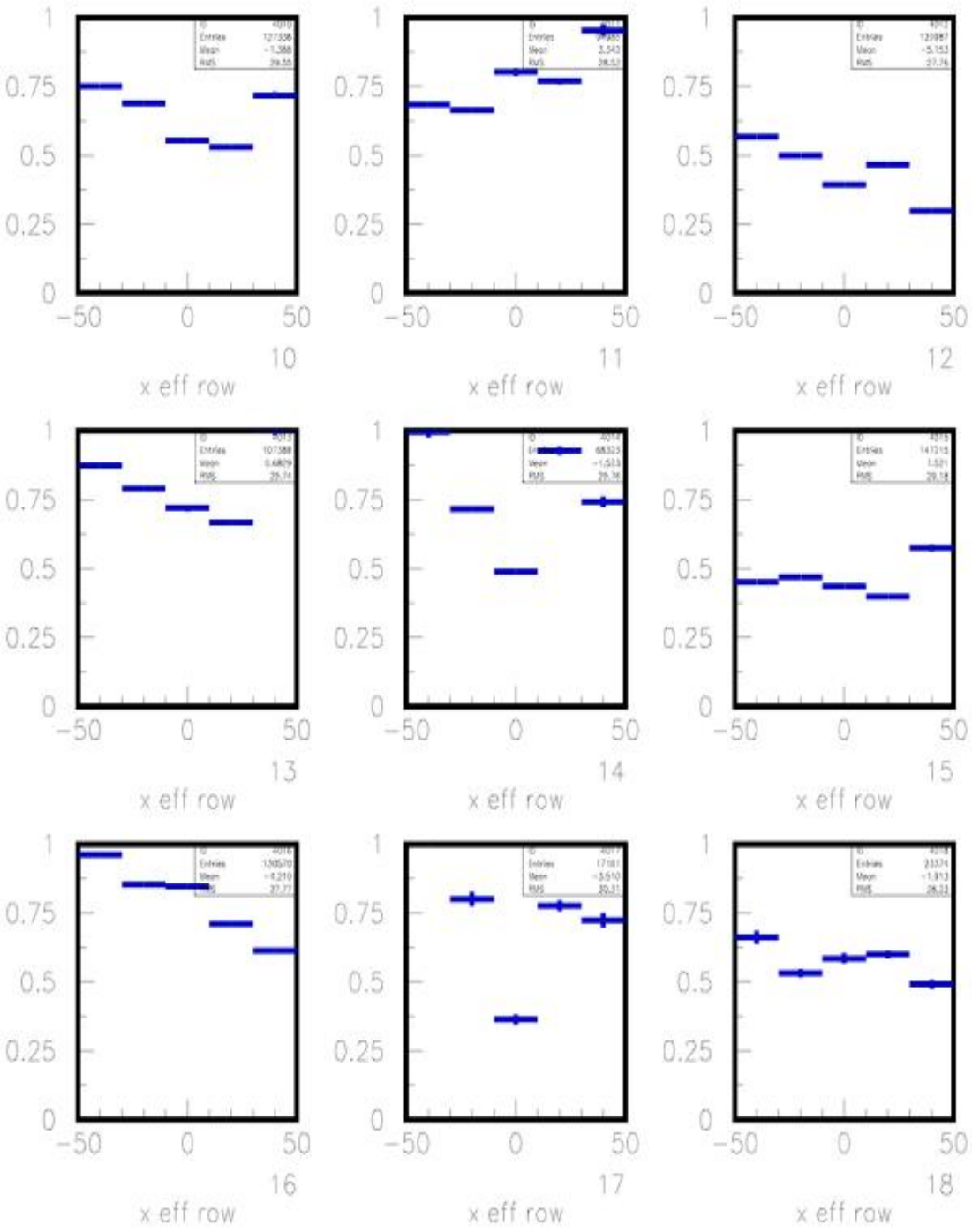

Figure 20. Per bar efficiency 10-18

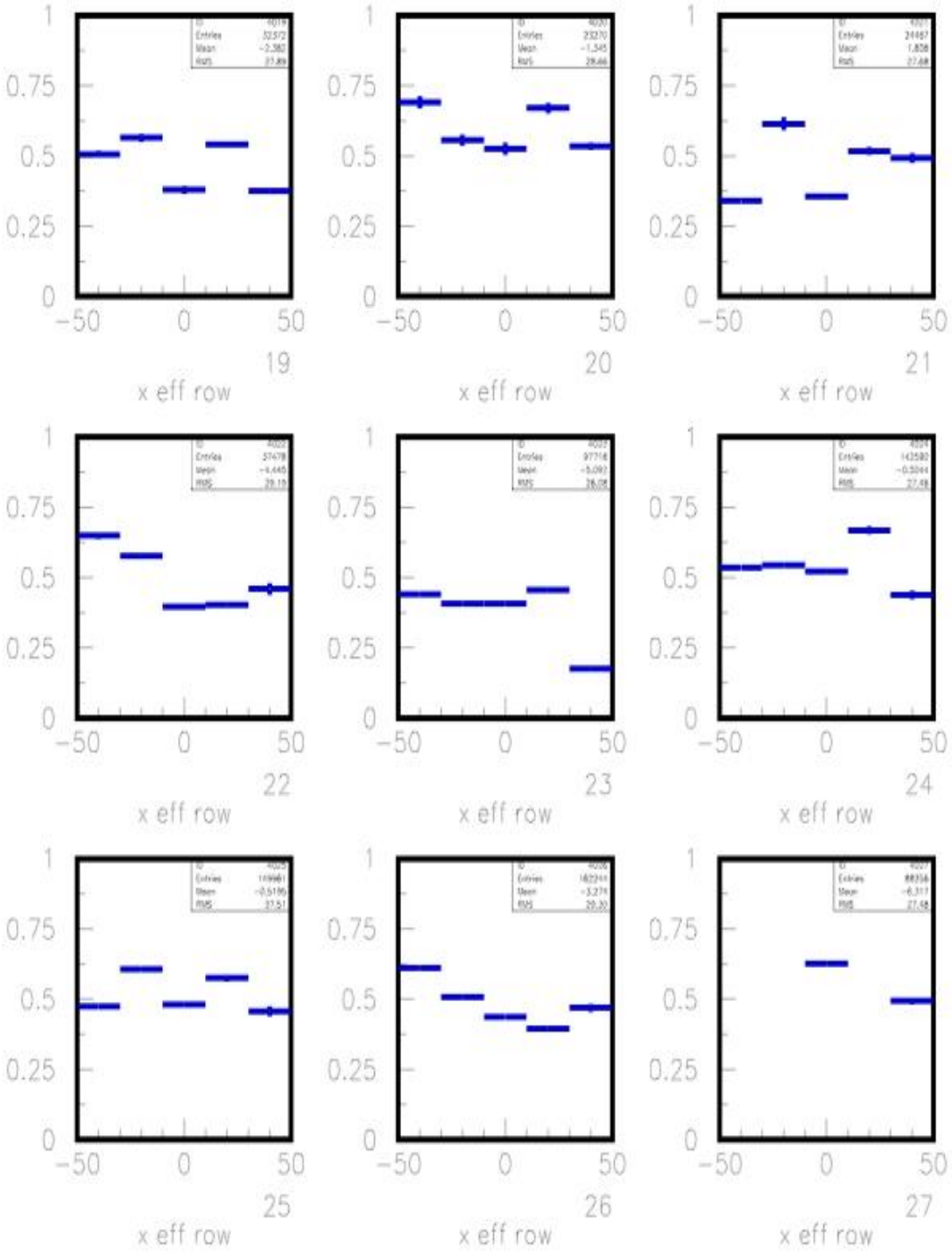

Figure 21. Per bar efficiency 19-27

At the same time efficiency is derived, both horizontal and vertical position resolution is determined. In comparing the difference between predicted positions of hits to experimental data, graphs with Gaussian fits will show the accuracy of the calculations. Figures 22 and 23 show the expected linear relationship between experimental and predicted values along the X and Y plane respectively along with their difference. These differences determine the position resolutions. Figure 24 graphs display the Gaussian curve and fit of the data. According to the data, the accuracy of the measurements comes within 2-3 cm. Figure 25 displays how the resolution barely changes across each bar from left to right. Figures 21 and 22 show resolution for particular bars. The Gaussian fit to these data sets give values within an acceptable range. Table 3 is a table of the recorded Gaussian sigma values for horizontal and vertical resolution.

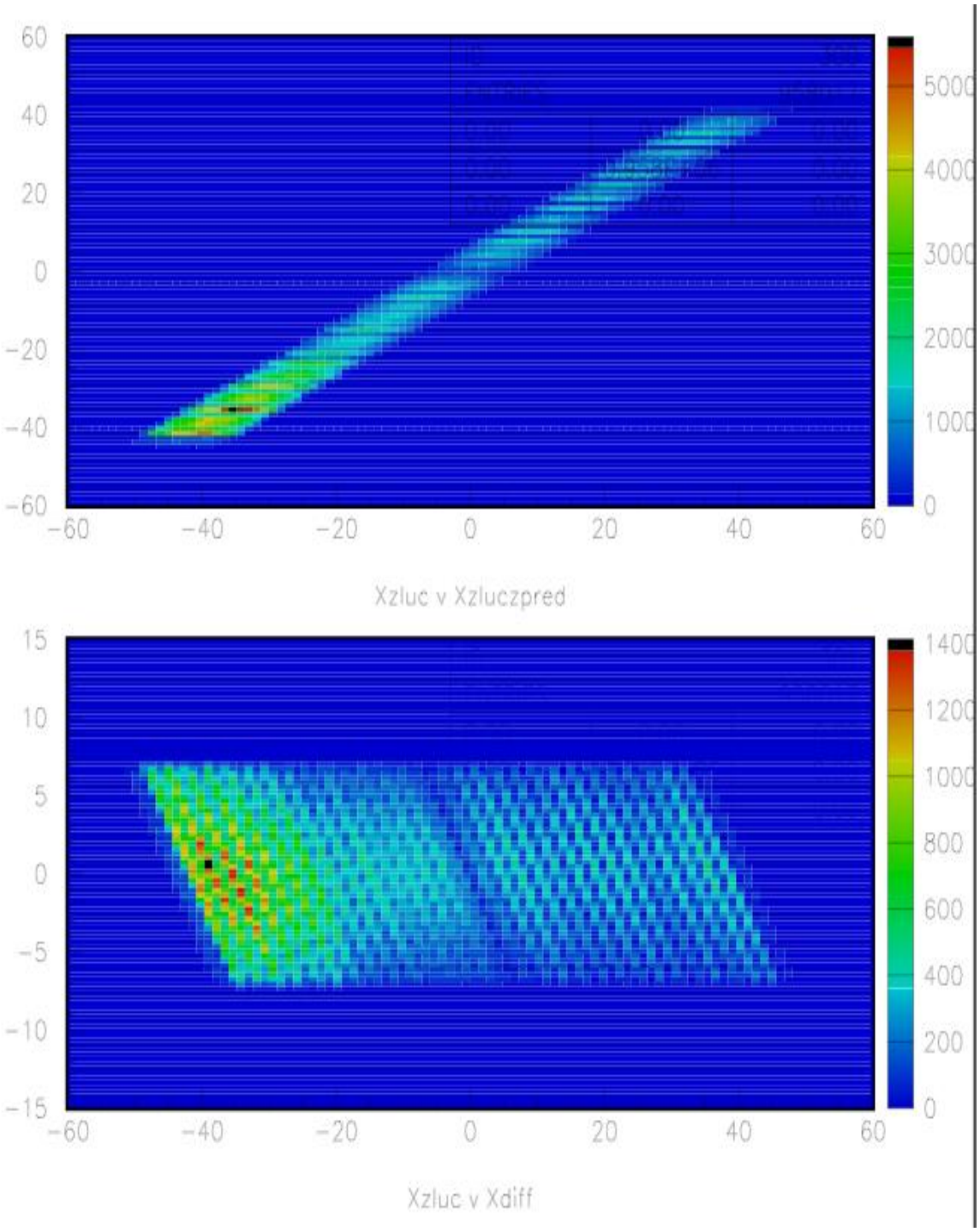

Figure 22. Lucite vs. predicted and Lucite vs. difference in X

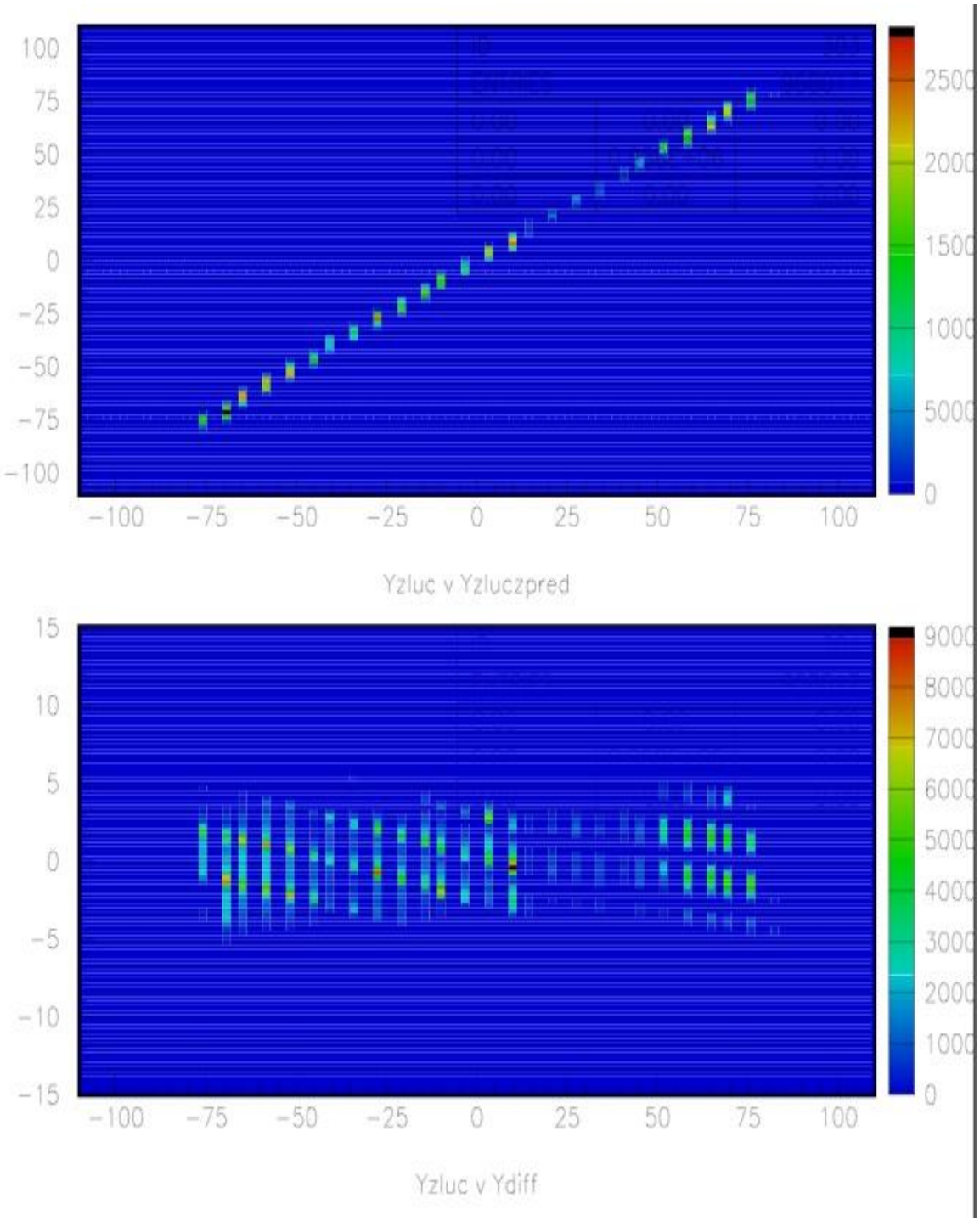

Figure 23. Lucite vs. predicted and Lucite vs. difference in Y

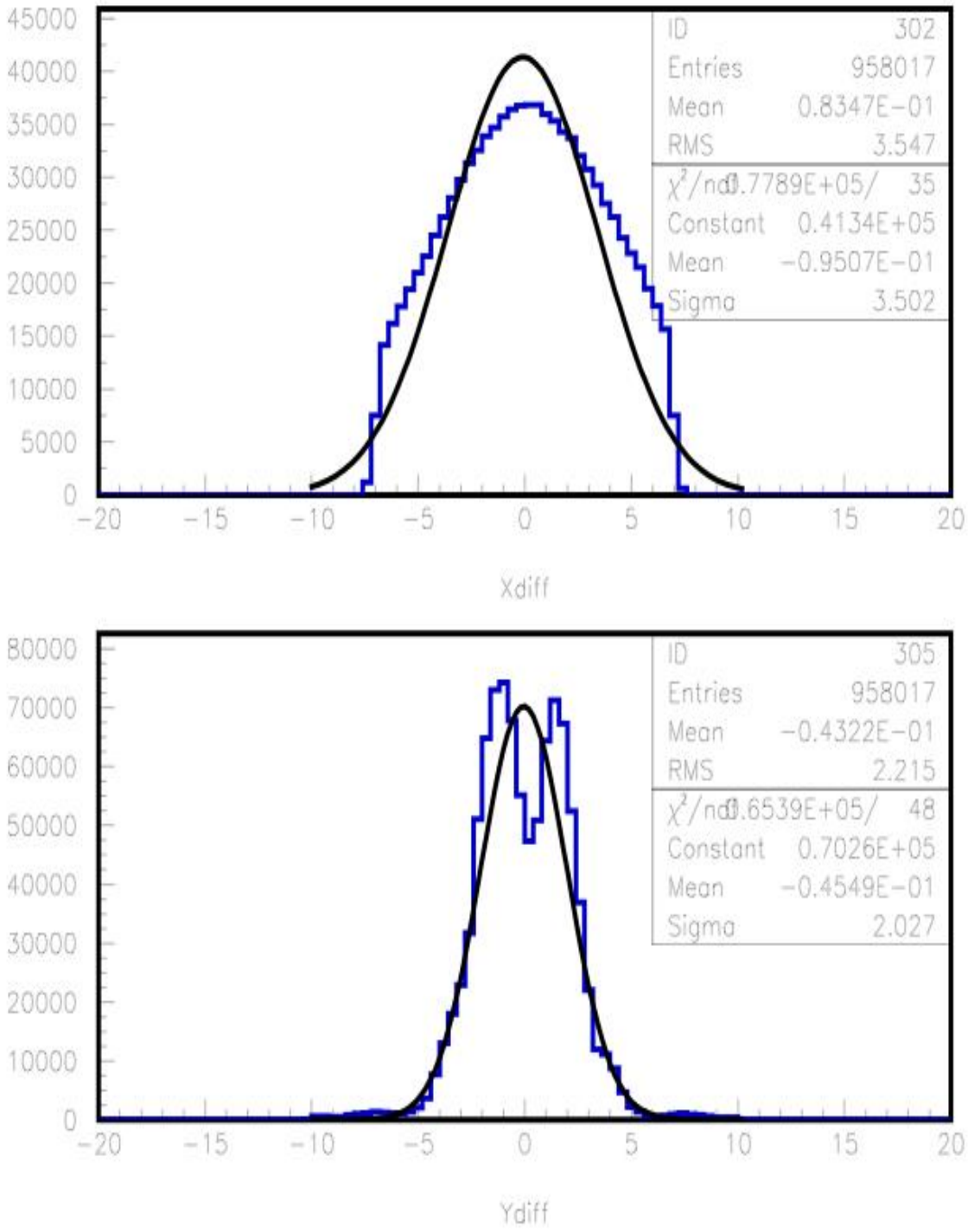

Figure 24. X and Y resolutions, fit with Gaussian distribution

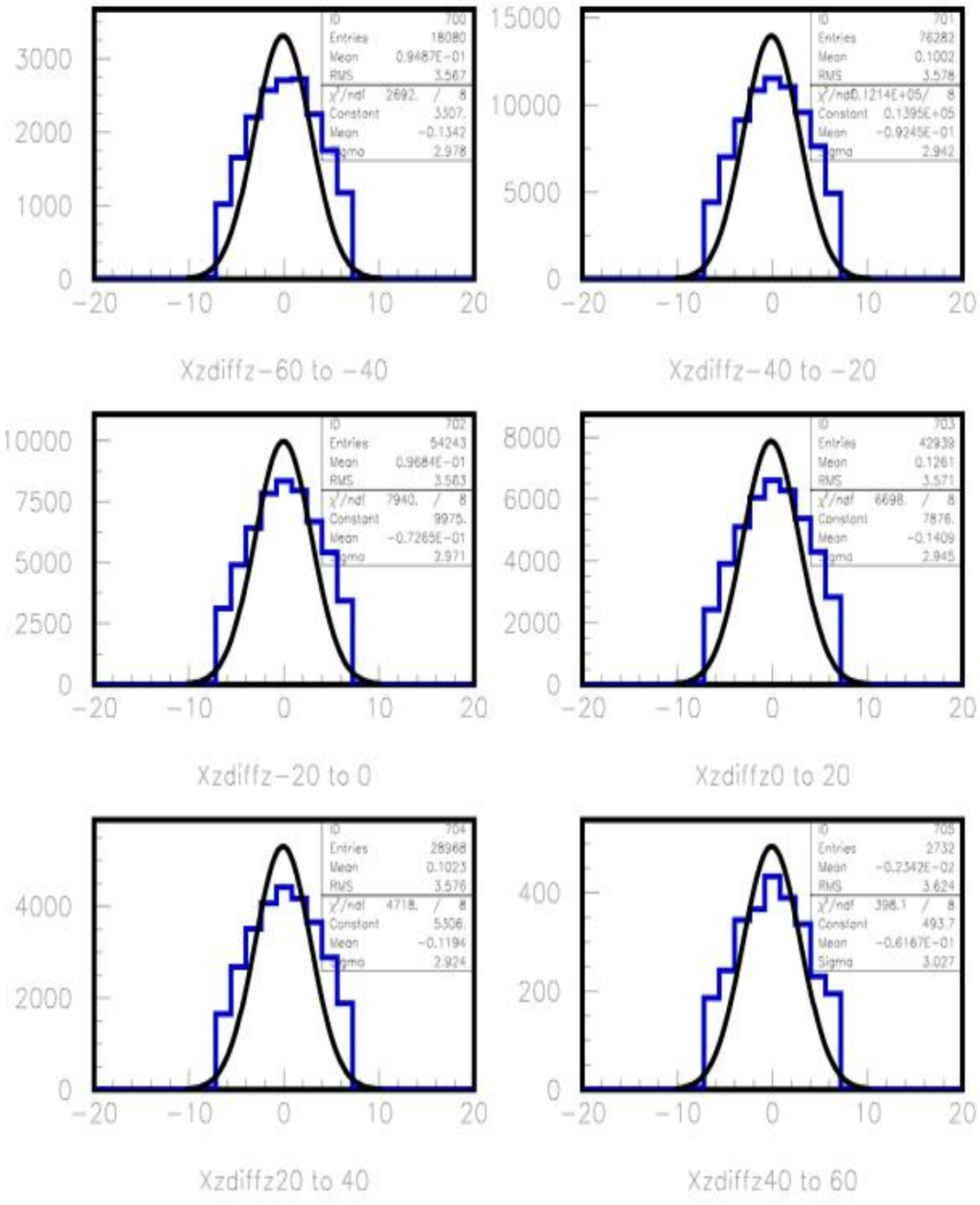

Figure 25. X resolution across bar

Table 3. Position resolutions

Bar	X sigma	Y sigma
1	4.153856	1.962967
2	3.133320	1.987096
3	3.224193	1.991519
4	2.996586	1.979017
5	3.217523	1.997089
6	2.905495	1.990290
7	2.918156	1.981054
8	3.115085	1.987691
9	2.929246	1.996075
10	3.167127	1.979932
11	3.113425	1.982781
12	3.194345	1.988271
13	3.246239	1.994629
14	2.999186	1.982475
15	3.181918	1.976021
16	2.853624	1.984797
17	3.320098	1.974930
18	3.759528	1.995985
19	3.154873	1.961484
20	3.052633	1.982178
21	3.032471	1.970079
22	3.435270	1.983833
23	3.169391	2.006595
24	3.220056	1.990546
25	3.159657	1.992576
26	3.290799	1.997454
27	3.145272	1.992837
28	3.955297	1.932010

CHAPTER 6

Conclusion

The Spin Asymmetries of the Nucleon Experiment (SANE) ran successfully at Jefferson (JLab). It is currently (as of March 2011) in the data analysis phase. Preliminary results for SANE's goals are the subject of many talks and presentations over the past year. Most current results concern the asymmetries $A_{\parallel}$ and $A_{\perp}$. Soon members of the analysis team plan to publish a few papers regarding the results. The Lucite Hodoscope was planned to be vital in the analysis phase of the experiment, but due to low efficiencies, many of the analysis codes did not involve the hodoscope. Further investigation is needed to include it in the final analysis of the experiment.

With global efficiencies around 56%, the Lucite could not serve as an adequate piece for getting tracking information. Certain areas of the bars failed in recording valid efficiency values. The process in finding the efficiencies was sound and confirmed preliminary results taken before the Lucite analysis code was written. More work can be done in order to understand why the Lucite Hodoscope did not meet efficiency expectations. For position resolution, the Lucite Hodoscope's data met expectations. With position resolution differences for X = 3.5 cm and Y = 2.0, the analysis code adequately determined location of each event. Further work on the Lucite Hodoscope should include investigating the efficiency through events with one PMT hit and a Monte Carlo simulation of the hodoscopes to compare with the experimental data.

BIBLIOGRAPHY

1. K. Abe, *et al.* [E143 Collaboration], *Phys. Rev.* **D58**, 112003 (1998).

2. P. L. Anthony, *et al.* [E155 Collaboration], *Phys. Lett.* **D458**, 529 (1998); P. L. Anthony, *et al.* [E155 Collaboration], *Phys. Lett.* **D553**, 18 (2003).

3. F. R. Wesselmann, *et al.* [E143 Collaboration], *Phys. Rev. Lett.* **98**, 132003 (2007), [nucl-ex/0608003].

4. N. Isgur, *Phys. Rev.* **D59**, 034013 (1999).

5. K. V. Dharmawardane, *et al.* [CLAS Collaboration], *Phys. Lett.* **D641**, 11 (2007).

6. S. Matsuda and T. Uematsu, *Nucl. Phys.* **B168**, 181 (1980).

7. M. Stratmann, *Z. Phys.* **C60**, 763 (1993).

8. X. Ji and P. Unrau, *Phys. Lett.* **B333**, 288 (1994).

9. J. S. McCarthy and X. Song, *Phys. Rev.* **D49**, 3169 (1994); **D50**, 4718 (1994) (Erratum).

10. L. Gamberg, H. Reinhardt and H. Weigel, *Phys. Rev.* **D55**, 6910 (1997).

11. M. Wakamatsu, *Phys. Lett.* **B487**, 118 (2000).

12. M. Gockeler, *et al. Phys. Rev.* **D49**, 054507 (2005).

13. E. Stein, *et al. Phys. Lett.* **B343**, 369 (1995).

14. I. Balitsky, *et al. Phys. Lett.* **B242**, 245 (1990); **B318**, 648 (1993) (Erratum).

15. H. Burkhardt, W. N. Cottingham, *Ann. Phys.* **56**, 453 (1970).

16. A. V. Efremov, E. Leader, and O. V. Teryaev, *Phys. Rev.* **D55**, 4307 (1997).

17. Saint Gobain. (2009) http://www.saint-gobain.com.

18. Photonis. (2009) http://www.photonis.com